View Online / Journal Homepage / Table of Contents for this issue
Dynamic Article Links

Organic & Biomolecular Chemistry

Cite this: *Org. Biomol. Chem.*, 2012, **10**, 7527

www.rsc.org/obc

PAPER

Theoretical insight into linear optical and two-photon absorption properties for a series of *N*-arylpyrrole-based dyes†

Xiao-Ting Liu,[a,b] Jing-Fu Guo,[c] Ai-Min Ren,*[a] Zhong Xu,[a] Shuang Huang[a] and Ji-Kang Feng[a]

Received 13th May 2012, Accepted 27th July 2012
DOI: 10.1039/c2ob25916h

Published on 30 July 2012 on http://pubs.rsc.org | doi:10.1039/C2OB25916H
Downloaded by University of California - San Diego on 01 September 2012

N-arylpyrrole-based dyes possessing excellent opto-electronic properties are promising candidates for two-photon fluorescence labeling materials. The systematic investigation of novel *N*-arylpyrrole derivatives is of great importance for both fine-tuning electronic spectra and designing two-photon absorption (2PA) materials. We thoroughly studied influences of the π-conjugated center and *N*-substituted pyrrole moieties on the linear optical and 2PA properties. Our results show that introducing *N*-arylpyrrole produces bathochromic-shifts of the absorption and emission bands and an enhancement of the 2PA cross section (δ_{max}), demonstrating that the electron-rich pyrrole moieties can efficiently increase intramolecular charge transfer. Substitution of fluorenyl with benzothiadiazole produces the lower energy gap, higher emission lifetime, red-shift of 2PA spectra and larger δ_{max}. The absorption and emission bands are highly dependent on the nature of the active building blocks. The aromatic rings attached to pyrrole can modulate the absorption peaks in the high energy and thus subtly modify the electronic properties.

Introduction

Two-photon absorption (2PA) is a nonlinear optical (NLO) process. The possibility of 2PA was first theoretically predicted by Maria Göppert-Mayer in 1931.[1] It is known that 2PA is related to the imaginary part of third order nonlinear susceptibility from a theoretical perspective. Only after the invention of a laser source in 1961 was the first experimental verification of the 2PA process demonstrated.[2] Nowadays, the surge of interest for synthesizing and characterizing two-photon active materials stems from their wide applications in diverse fields, such as microscopy,[3] three-dimensional (3-D) micro-fabrications,[4] 3-D data-storage,[5] optical power limiting,[6] photo-dynamic cancer therapy,[7] up-converted lasing,[8] and two-photon excited fluorescence (TPEF) imaging,[9] *etc.* This, in turn, leads to the search for adequate functional materials with high 2PA cross sections (δ_{max}).[10] Thanks to their inherent modularity and potentially high 2PA response, conjugated organic molecules are of particular interest. Most explored and efficient 2PA dyes can be described as symmetric D–π-D, dipolar D–π-A, quadrupolar D–π-A–π-D (A–π-D–π-A), and multipolar star-shaped structures (D = Donor, A = Acceptor).[11–14] The 2PA cross section of a molecule depends upon many factors such as the dimensionality of the charge-transfer network, push–pull strength, the electronic coupling, and the conjugation length. Some times, solvent also plays a dominant role in deciding the net cross section value.

The theoretical and experimental techniques can provide the 2PA cross section of a compound at a desirable wavelength. However, to the best of our knowledge, the experimental measurement of δ_{max} is always a difficult task and the net δ_{max} value depends on many factors.[15] These factors include the experimental technique used, the chosen excitation wavelength, spatial and temporal fluctuation of the laser beam, multiple reflection effect and time duration of the pulsed laser source. A slight variation of any of these factors can change δ_{max} by an order of magnitude.[16] Therefore, theoretical simulations are often viewed as important tools to evaluate the 2PA cross section of the target molecule and in the development of more suitable 2PA materials prior to the experimental verification. This will not only help us develop a new design strategy but also understand the underlying mechanism of the 2PA activity of a molecule.

In the past decades, the employment of π-excessive or deficient heterocycles in the construction of novel fluorophores has shown the result of an increased intramolecular charge transfer (ICT), as well as enhanced two-photon absorption.[17–20] Pyrrole is one of the strongest donor heteroaromatics and

[a]*State Key Laboratory of Theoretical and Computational Chemistry, Institute of Theoretical Chemistry, Jilin University, Changchun, 130023, People's Republic of China. E-mail: aimin_ren@yahoo.com*
[b]*State Key Laboratory of Rare Earth Resource Utilization, Changchun Institute of Applied Chemistry, Chinese Academy of Sciences, Changchun, 130022, People's Republic of China*
[c]*School of Physics, Northeast Normal University, Changchun, 130021, People's Republic of China*

† Electronic supplementary information (ESI) available: The contribution of electron density (%) and contour surfaces of the frontier molecular orbitals relevant to the maximal OPA and 2PA for the studied molecules. See DOI: 10.1039/c2ob25916h

Published on 30 July 2012 on http://pubs.rsc.org | doi:10.1039/C2OB25916H
Downloaded by University of California - San Diego on 01 September 2012

possesses attractive chemical and physical properties for the construction of 2PA molecules. By introducing the electron-rich pyrrole ring as the building block to the various types of compounds, large δ_{max} have been obtained by the Marder groups.[19,21–23] In the reported references, the electron-rich pyrrole ring was functionalized at the α-position to build the 2PA conjugated chromophores, which demonstrated enhanced second-order nonlinear optical effects in comparison with their analogues bearing furan or thiophene groups.[24] Interestingly, Li *et al.* have recently synthesized some new pyrrole-containing molecules with the modification of fluorenylene and phenylene units connected to pyrrole, and triphenylamine group together with phenyl linked to pyrrole through the C–N single bond.[25] And these *N*-arylpyrrole-based chromophores exhibit excellent opto-electronic behavior, especially high stability, high fluorescent quantum yields, and large 2PA cross sections, as well as good solubility relative to their analogs, which may be ascribed to the suspension structure facilitating multiple pathways for intramolecular electronic and photonic transfer. Exactly, their outstanding properties qualify them as promising biological fluorescent probes.[9,26–30] To fully realize the substantial potential of two-photon excitation of the fluorescent probes, it is important to know their 2PA spectra and 2PA cross sections. Here, we give an accurate theoretical study of linear optical absorption and fluorescence, as well as 2PA properties for *N*-arylpyrrole-based dyes. The quantum chemical calculation can in depth elucidate the dependence of band gaps, as well as the origin of linear and nonlinear optical properties. We believe that this detailed computational investigation performed on a series of new *N*-arylpyrrole-based molecules will contribute to the overall understanding of structure–properties relationships and stimulate further research work towards obtaining the most promising 2PA biological fluorescent dyes.

Theoretical methodology

B3LYP was implemented for ground-state geometry optimizations of the *N*-arylpyrrole-based derivatives, since it is known to give good results for organic molecules.[31] At the same level, frequency calculations were carried out to verify the identity of each stationary point as a minimum. Vertical singlet excitation energies were calculated on the basis of the optimized systems using the time-dependent (TD) formalism in combination with the B3LYP, CAM-B3LYP[32] and M062X[33] functionals. The detailed data including maximum one-photon absorption (OPA) wavelengths (λ^{O}_{max}), and corresponding oscillator strengths (f), as well as the experimental data for molecules **P1** and **P2** are collected in Table 1. As shown, the maximum values of UV/Vis absorption obtained by B3LYP are longer by 100 nm than the experimental results.[25] As a consequence, the hybrid functional M062X and the long-range corrected functional CAM-B3LYP can provide reasonable singlet state energies. In the present work, the one-photon absorption and emission properties, as well as the energies of frontier orbitals are performed at the CAM-B3LYP/6-31G* level. The CAM-B3LYP functional used here can better describe long range charge distribution modifications, which is important for accurately determine the charge transfer transitions of the investigated dyes. All the calculations were performed by utilizing Gaussian 09 program suite.[34]

Table 1 One-photon absorption spectra for **P1** and **P2** with different TD-DFT functionals

	P1		**P2**	
Method	λ^{O}_{max}/nm	f	λ^{O}_{max}/nm	f
B3LYP/6-31G*	551.9	3.95	551.9	3.97
M062X /6-31G*	447.5	4.78	447.5	4.83
CAM-B3LYP/6-31G*	444.5	4.82	444.5	4.87
Experimental data[25]	447		452	

The OPA properties of all molecules were also predicted by means of the Zerner's intermediate neglect of differential overlap (ZINDO) program[35] including single and double electronic excitation configuration interaction.

The 2PA process corresponds to simultaneous absorption of two photons. The 2PA efficiency of an organic molecule, at optical frequency $\omega/2\pi$, can be characterized by the 2PA cross-section $\delta(\omega)$. It is proportional to the imaginary part of the third-order polarizability $\gamma(-\omega;\omega,-\omega,\omega)$ by:[36,37]

$$\delta(\omega) = \frac{3\hbar\omega^2}{2n^2c^2\varepsilon_0} L^4 \mathrm{Im}[\gamma(-\omega;\omega,-\omega,\omega)] \qquad (1)$$

where $\gamma(-\omega;\omega,-\omega,\omega)$ is the third-order polarizability, $\hbar\omega$ is the energy of incoming photons, c is the speed of light, ε_0 is the vacuum electric permittivity, n denotes the refractive index of medium and L corresponds to the local-field factor. In the calculations presented here, n and L are set to 1 because of isolated molecule in vacuum. The components of the third-order polarizability γ can be evaluated by a sum-over-states (SOS) expression. A general expression of γ is given by ref. 38 and 39. It depends on the transition frequencies ω_{ij}, transition dipole moment μ_{ij}, and the coherence damping rate Γ_{ij} between the state i and j state.

To compare the calculated $\delta(\omega)$ value with the experimental value measured in solution, the damping factor (Γ_K) of excited state K in the SOS expression is set to 0.16 eV.[40,41] And the orientationally averaged (isotropic) value of γ is evaluated, which is defined as

$$\langle\gamma\rangle = \frac{1}{15}\sum_{i,j}(\gamma_{iijj} + \gamma_{ijij} + \gamma_{ijji}) \quad i,j = x,y,z \qquad (2)$$

Taking the imaginary part of $<\gamma>$ value into the expression (1), we can obtain $\delta(\omega)$ in comparison with the experimental value.

In this work, the properties of electronic excited states were obtained by single and double electronic excitation configuration interaction (SDCI) using the ZINDO program. Moreover, the transition energies and transition moments were also obtained. Then, the FTRNLO program compiled by our group was used to calculate the second hyperpolarizability and two-photon absorption cross section. The calculated 2PA cross-sections of all molecules included the contributions from 300 lowest-lying excited states which were sufficient for the convergence of $\delta(\omega)$.

 This journal is © The Royal Society of Chemistry 2012

Downloaded by University of California - San Diego on 01 September 2012
Published on 30 July 2012 on http://pubs.rsc.org | doi:10.1039/C2OB25916H

Results and discussions

Molecular design and geometry optimization

The studied molecular structures are presented in Fig. 1. We performed the calculations on a series of model compounds (**P1** and **P2**) for dyes **PL-1** and **PL-2**[25] where the aliphatic side chains were all replaced by methyl groups for the sake of simplification. In fact, the aliphatic side chains only improve the molecular solubility and the simplification has little effect on electronic spectra and nonlinear optical response.[41] Chromophores **P1**, **P3**, **P5**, **P6**, and **P9** with the same *N*-alkylpyrrole moiety, yet feature fluorenylene (Flu), dimethoxyphenylene (Ph1), carbazole (Car), pyrene (Pyr), and benzothiadiazole (BTD) units as the center moieties. Molecules **P1**, **P2**, and **P8** were constructed by introducing triphenylamine (TPA), phenylene (Ph2), and boron-dipyrromethene (Bod) units together with phenyl linked to pyrrole through the C–N single bond. The similar modification is made for **P3**, **P4**, and **P7**. The difference between the two series is that the former contains the Flu center and the latter possesses the Ph1 moiety. In addition, the *cis*- and *trans*-isomers were taken into account as an example of molecule **P1**. Among all the studied chromophores, **P1**–**P4** are model compounds for the reported dyes in ref. 25, but **P5**–**P9** are our constructed molecules. The designed *N*-alkylpyrrole-based chromophores belong to the D–π-D type, in which triphenylamine acts as the electron donor and, the center and *N*-alkylpyrrole moieties as the π-conjugated bridge. Boron-dipyrromethene and benzothiadiazole building blocks induced are expected to bring good 2PA properties.

The geometric structures were fully optimized with no symmetry constraint using the Gaussian 09 program with 6-31G* basis set at the B3LYP level. For the sake of confirming the stability of the optimized structures, the harmonic vibrational frequencies upon the optimized structures were evaluated at the same level, and no imaginary frequency was found. The optimized ground-state geometries of all molecules are described in Fig. 2. As shown, the central frameworks of all chromophores remain nearly planar except for **P7** and **P8** featuring boron-dipyrromethene moieties whose central cores are slightly twisted. The geometry changes are conceived to have a substantial influence on the electro-optical properties.

Electronic structures

The energies of some frontier orbitals (four occupied orbitals, four unoccupied orbitals and energy gap (ΔE_{H-L}) between the highest occupied molecular orbital (HOMO) and the lowest unoccupied molecular orbital (LUMO)) obtained by CAM-B3LYP/6-31G*, are shown schematically in Fig. 3. The energy of HOMO increases with different central substitutes, that is, **P6** (−5.40 eV) < **P1** (−5.31 eV) < **P5** (−5.29 eV) < **P3** (−5.22 eV) < **P9** (−5.21 eV). However, the energy of LUMO is decreased in the order of **P3**, **P5**, **P6**, **P1**, and **P9**. This means that introducing pyrene in the central core leads to the reduction of HOMO energy and the enhancement of LUMO energy and in turn increased ΔE_{H-L}. But molecule **P9** features the highest HOMO energy and the lowest LUMO energy, as well as the lowest energy gap. This reveals that **P9** is the most easily oxidized by many oxidants. Replacement of triphenylamine and phenylene with boron-dipyrromethene units makes the LUMO energy decreased and ΔE_{H-L} smaller whatever the central moiety is a fluorenylene or dimethoxyphenylene unit.

One-photon absorption and emission properties

On the basis of the optimized geometries, the OPA properties of all chromophores were calculated by the TD CAM-B3LYP/6-31G* method. The detailed data involving maximum absorption wavelengths (λ^{O}_{max}), and corresponding oscillator strengths (f), as well as the experimental values are tabulated in Table 2. As compared, the maximum values of UV/Vis absorption for **P1**, **P2**, **P3**, and **P4** are 444.5, 444.5, 435.6, and 465.9 nm, which are in good agreement with the experimental data (447, 452, 469, and 469 nm), respectively.[25] For molecule **P1**, the OPA properties of both its *trans*- (**P1-a**) and *cis*- isomers (**P1**) were calculated and the results clearly suggest that the *trans*- and *cis*-isomers possess almost the same OPA properties. Herein we will use the *cis*-form of all molecules with the suspended configuration in the following discussion. Moreover, to certify the influence of the pyrrole moieties on the OPA properties, we also calculated the λ^{O}_{max} value of **P1flu** without pyrrole rings at the π-system relative to **P1**. From Table 2, adding *N*-arylpyrrole moieties produces a large bathochromic-shift of 30 nm, which

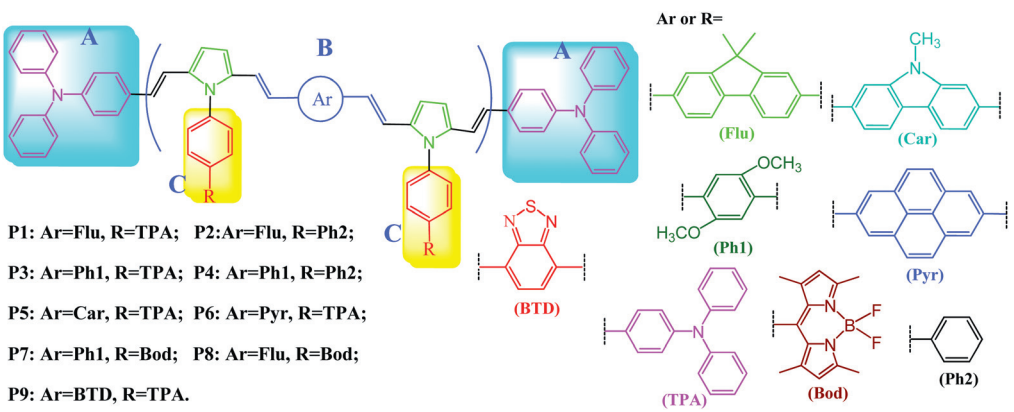

Fig. 1 Molecular structures of all the *N*-arylpyrrole-based chromophores.

Published on 30 July 2012 on http://pubs.rsc.org | doi:10.1039/C2OB25916H
Downloaded by University of California - San Diego on 01 September 2012

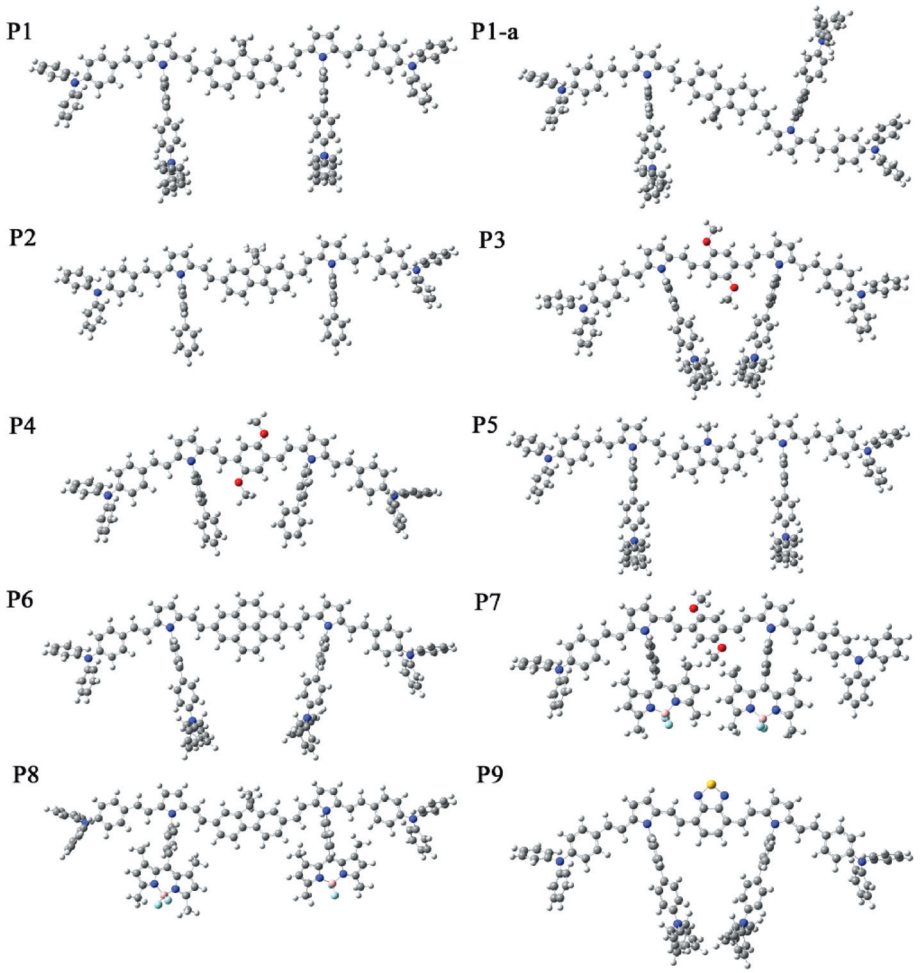

Fig. 2 The optimized ground state geometries of the molecules studied.

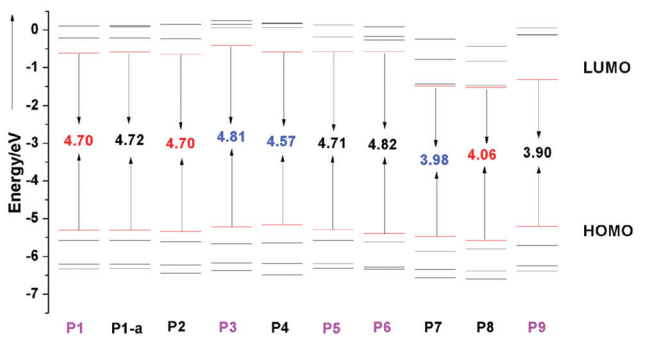

Fig. 3 Frontier orbital energies of fluorophores at the CAM-B3LYP/6-31G(d) level.

demonstrates that the electron-rich pyrrole ring is efficient to increase the intramolecular charge transfer, as well as to enhance optical properties.

As clearly shown in Table 2, all pyrrole fluorophores exhibit an intense absorption band ranging from 425 to 580 nm. The result displays that the central groups, and the substitution at the phenyl attached to the pyrrole ring can finely tune the linear optical property. Substitution of the fluorenyl center with the benzothiadiazole substituent produces a red-shift by 134 nm of the absorption band with respect to **P1**, but for molecules **P3**, **P5**, and **P6**, their absorption spectra are hypsochromically shifted, which is just corresponding to the ΔE_{H-L} above. In particular, introducing pyrene in the center leads to the largest blue-shift of the absorption band. This implies that the λ^{O}_{max} values can be determined by the central core. But the peak (about 290 nm) in the absorption spectra of the five molecules **P1**, **P3**, **P5**, **P6**, and **P9** can be ascribed to the triphenylamine groups which was connected to pyrrole together with phenyl one through the C–N single bond as an auxiliary donor group. Interestingly, **P1**, **P2**, and **P8** exhibit similar absorption maximum wavelengths at about 440 nm. And for **P3**, **P4**, and **P7** bearing bismethoxyphenylene, their λ^{O}_{max} values were slightly different. But in the high energy region, replacement of triphenylamine and phenylene with boron-dipyrromethene units makes the λ^{O}_{max} value a significant bathochromic-shift. For example, the middle peaks of **P1**, **P2**, and **P8** are 295.9, 276.0, and 415.3 nm, and the corresponding values are also predicted for **P3**, **P4**, and **P7** (292.8, 276.8, and 421.5 nm), respectively. Namely, the spectra in the high energy range could be modulated by the linkage of different R groups, providing another strategy to subtly modify the electronic properties of the chromophores. Moreover, from Table 2, it can be found that the transition

 This journal is © The Royal Society of Chemistry 2012

View Online

Table 2 One-photon absorption and excitation properties (TDDFT)[a]

Mol.	λ^{O}_{max}/nm	f	Transition character	λ^{E}_{max}/nm	E_{Flu}/eV	f^{E}	Transition character	τ/ns
P1	444.5	4.82	$S_0 \rightarrow S_1(H) \rightarrow (L)35\%$	488.6	2.54	4.74	$S_1 \rightarrow S_0(H) \rightarrow (L)39\%$	0.76
	295.9	1.21	$S_0 \rightarrow S_9(H-2) \rightarrow (L+1)9.5\%$	517[b]				
	447[b]							
P1-a	442.9	4.65	$S_0 \rightarrow S_1(H) \rightarrow (L)35\%$	487.2	2.55	4.58	$S_1 \rightarrow S_0(H) \rightarrow (L)38\%$	0.78
	299.0	1.73	$S_0 \rightarrow S_8(H-4) \rightarrow (L+2)20\%$					
			$(H-3) \rightarrow (L+3)19\%$					
P1flu	414.3	3.91	$S_0 \rightarrow S_1(H) \rightarrow (L)38\%$	466.7	2.66	3.92	$S_1 \rightarrow S_0(H) \rightarrow (L)41\%$	0.83
P2	444.5	4.87	$S_0 \rightarrow S_1(H) \rightarrow (L)35\%$	488.3	2.54	4.79	$S_1 \rightarrow S_0(H) \rightarrow (L)39\%$	0.75
	276.0	0.26	$S_0 \rightarrow S_{14}(H-2) \rightarrow (L+11)13\%$	523[b]				
	452[b]		$(H-1) \rightarrow (L+10)12\%$					
P3	435.6	3.64	$S_0 \rightarrow S_1(H) \rightarrow (L)39\%$	527.9	2.35	3.68	$S_1 \rightarrow S_0(H) \rightarrow (L)43\%$	1.14
	292.8	0.76	$S_0 \rightarrow S_8(H-3) \rightarrow (L+3)27\%$	554[b]				
	469[b]							
P4	465.9	3.84	$S_0 \rightarrow S_1(H) \rightarrow (L)40\%$	527.3	2.35	3.76	$S_1 \rightarrow S_0(H) \rightarrow (L)43\%$	1.11
	276.8	0.24	$S_0 \rightarrow S_{14}(H-1) \rightarrow (L+10)14\%$	551[b]				
	469[b]		$(H-2) \rightarrow (L+10)14\%$					
P5	443.4	4.85	$S_0 \rightarrow S_1(H) \rightarrow (L)35\%$	485.5	2.55	4.78	$S_1 \rightarrow S_0(H) \rightarrow (L)38\%$	0.74
	295.6	1.29	$S_0 \rightarrow S_{10}(H-3) \rightarrow (L+3)11\%$					
P6	428.2	5.03	$S_0 \rightarrow S_1(H) \rightarrow (L)33\%$	461.9	2.68	5.00	$S_1 \rightarrow S_0(H) \rightarrow (L)35\%$	0.64
	296.9	1.04	$S_0 \rightarrow S_{11}(H-3) \rightarrow (L+3)9.4\%$					
P7	454.2	2.36	$S_0 \rightarrow S_1(H) \rightarrow (L+2)36\%$	522.7	2.37	3.04	$S_1 \rightarrow S_0(H) \rightarrow (L+2)42\%$	1.35
	421.5	2.54	$S_0 \rightarrow S_3(H-4) \rightarrow (L)23\%$					
			$(H-3) \rightarrow (L+1)21\%$					
P8	440.9	3.48	$S_0 \rightarrow S_1(H) \rightarrow (L+2)32\%$	489.2	2.53	3.72	$S_1 \rightarrow S_0(H) \rightarrow (L+2)39\%$	0.97
	415.3	1.78	$S_0 \rightarrow S_3(H-5) \rightarrow (L)24\%$					
			$(H-3) \rightarrow (L+1)17\%$					
P9	578.6	2.06	$S_0 \rightarrow S_1(H) \rightarrow (L)44\%$	679.4	1.82	1.73	$S_1 \rightarrow S_0(H) \rightarrow (L)46\%$	4.03
	391.2	2.03	$S_0 \rightarrow S_3(H) \rightarrow (L+1)34\%$					
	297.0	1.48	$S_0 \rightarrow S_{13}(H-4) \rightarrow (L+3)19\%$					

[a] H and L denote HOMO and LUMO, respectively. [b] Experimental data.[25]

Published on 30 July 2012 on http://pubs.rsc.org | doi:10.1039/C2OB25916H
Downloaded by University of California - San Diego on 01 September 2012

character of all chromophores except for molecules **P7** and **P8** in the low-energy region is from valence HOMO to LUMO. The transitions of **P7** and **P8** in low-energy region cause from HOMO to LUMO + 2 due to the presence of boron-dipyrromethene substituent groups. Orbital analysis reveals that the π–π* transitions occur typically at the π-conjugated systems (*cf.*, Fig. S1, ESI†). And the HOMO possesses an anti-bonding character and the LUMO shows a bonding character between the subunits. The electronic structures present a high degree of coplanarity in the π-system, which should be a beneficial factor for communication between the donor and conjugated bridge. But in the high-energy region, the electronic transition is actually complicated. In particular, the *N*-alkylpyrrole moieties take part in the intramolecular charge transfer. The contribution of the fragments to the frontier orbitals associated with the OPA is discussed by the local density of the states (LDOS) analysis (Table S1, ESI†). For clarity, the molecule is divided into three parts, namely the triphenylamine terminal groups (A), π-center framework (B), and *N*-substituted pyrrole moieties (C) (*cf.* Fig. 1). As shown in Table S1 and Fig. S1,† the electronic density distribution of HOMO and LUMO for all molecules except for molecules **P7** and **P8** (HOMO and LUMO + 2) mainly locates about 80% on the π-center system. However, the contribution of C (the *N*-alkylpyrrole moieties) is very little. This further indicates that the intense absorption is determined by the center. According to the LDOS analysis, the contribution of A in molecule **P1** to HOMO − 2 is 74.1%, while the contribution of B to LUMO + 1 is 63.8%, indicative of ICT from A (electron-donating groups) to B (the central framework). For molecules **P2** and **P4**, corresponding to the high energy peak consisting of HOMO − 2 → LUMO + 10, the contribution of A to HOMO − 2 is about 74%, while the contribution to LUMO + 10 is above 99%, giving rise to an obvious increase of electronic density for triphenylamine groups. Remarkably, for other molecules, the contribution of *N*-alkylpyrrole moieties to the orbitals is above 90%, implying the substituents attached to the pyrrole ring can modulate the optical properties in high energy region.

For the emission spectra, the calculations for molecules **P1**, **P2**, **P3**, and **P4** are 488.6, 488.3, 527.9, and 527.3 nm, respectively. The results are in reasonable agreement with the experiment data 517, 523, 554, and 551 nm, respectively. As clearly shown in Table 2, the strongest emission peaks of all fluorophores are assigned to the π–π* type, arising from S_1. All transitions are caused from HOMO to LUMO, except for molecules **P7** and **P8** (HOMO → LUMO + 2). All pyrrole fluorophores emit strong luminescence in the range of 488–680 nm with the largest oscillator strength from the lowest excited state. And the Stoke's shift between the absorption and emission bands ranges from 40 to 100 nm. From Table 2, it can be found that **P1**, **P2**, and **P8** exhibit similar emission band at about 490 nm, while the maximum emission wavelengths of **P3**, **P4**, and **P7** (about 520 nm) are the same. The replacement of the fluorenylene unit by dimethoxyphenylene results in a red-shift of 30 nm, and the decrease of fluorescent oscillator strength. The different emission behavior is similar to the difference in their absorption spectra. The trend suggests although the fluorenylene moiety possesses the larger conjugation space, the dimethoxyphenylene space is much easier to communicate with other moieties than the

Downloaded by University of California - San Diego on 01 September 2012
Published on 30 July 2012 on http://pubs.rsc.org | doi:10.1039/C2OB25916H

fluorenylene unit which may hamper its communication to some degree. Substitution of the fluorenyl center with the benzothiadiazole constructing block produces a red-shift by 191 nm of the emission band and the lowest f^{E}, but for molecule **P6** featuring pyrene as the building block, its emission spectra are hypsochromically-shifted by 26.7 nm. However, introducing pyrene in the center leads to the largest f^{E} among all molecules. This implies that the λ^{E}_{max} values are highly dependent on the nature of the active building blocks.

Table 2 also lists the emission lifetimes (τ) calculated for spontaneous emission by using the Einstein transition probabilities according to the formula (in au):[42,43]

$$\tau = \frac{c^3}{2(E_{Flu})^2 f^{E}} \quad (4)$$

The quantum yield (ϕ) is given by the following expression:[44]

$$k_r = \frac{1}{\tau} \quad \phi = \frac{k_r}{k_r + k_{nr}}$$

where c is the velocity of light, E_{Flu} is the transition energy, f^{E} is the oscillator strength, K_r is the rate of radiative decay, and K_{nr} is the nonradiative decay rate. The data of E_{Flu}, τ and f^{E} are also showed in Table 2. The calculated emission lifetimes of all molecules are in the same order of magnitude (ranging from 0.64 to 4.03 ns). Thus, replacement of fluorenylene by dimethoxyphenylene leads to the reduction of the emission lifetimes, such as **P1** (0.76 ns) < **P3** (1.14 ns), **P2** (0.75 ns) < **P4** (1.11 ns), and **P8** (0.97 ns) < **P7** (1.35 ns). According to the literature,[25] the quantum yields of **P1** (62.4%) and **P2** (66.3%) are higher than those of **P3** (41.0%) and **P4** (38.2%). In comparison with the calculated and experimental results, we can approximately neglect the change of the nonradiative decay rate aiming to analyze the change trend of ϕ. As displayed in Table 2, it could be easily seen that **P6** bearing pyrene shows the strongest emission and the shortest emission lifetime, indicative of its highest quantum yield. In contrast, introducing a benzothiadiazole substituent as the building block (**P9**) produces the reduction of the emission oscillator strength and the enhancement of the emission lifetime with respect to **P1**. Interestingly, **P1**, **P2**, and **P8** (or **P3**, **P4**, and **P7**) exhibit slight differences in the emission lifetimes, demonstrating that the aromatic rings attached to pyrrole through the C–N single bond have little influence on the fluorescence quantum yield.

In order to consider the effect of double electronic excitation configuration interaction on transition energies, the OPA properties of all chromophores were also calculated by the ZINDO/SDCI method on the basis of the optimized geometric structures. The corresponding data are collected in Table 3. As shown, the λ^{O}_{max} values of compounds **P1**, **P2**, **P3**, and **P4** obtained by ZINDO/SDCI (469.0, 467.8, 471.2, and 479.4 nm) are well in line with the experimental data (447, 452, 469, and 469 nm).[25] That is to say, ZINDO can also describe this system very well. This good result makes us confident for the theoretical prediction to 2PA properties of the fluorophores by ZINDO/SOS. As shown in Table 3, it has to be noted that the ZINDO method predicts the similar changing trends to TD-DFT//CAM-B3LYP/6-31G* above mentioned. Specially, the transition character analysis of the ground and excited states for all molecules displays that the lowest and strongest absorption band is composed of the HOMO → LUMO electronic transition except for **P7** and **P8** (mainly HOMO → LUMO + 2). This is in beautiful accordance with the transition assignment of the CAM-B3LYP functional.

Since the solvent effect is crucial for a direct comparison between experiment and calculation, the OPA properties calculation in THF is performed by ZINDO/SDCI *via* PCM as well. As can be seen in Table 3, comparing the results in vacuum and in THF, it is evident that the influence of the solvent is very slight, with the largest derivation of 14 nm.

Two-photon absorption properties

The two-photon absorption cross sections of all fluorophores are determined over a broad spectral range of 600–1200 nm by utilizing the ZINDO-SOS program. The maximum 2PA cross section (δ_{max}), 2PA maximum wavelength (λ^{T}_{max}), transition nature, and the experimental data are summarized in Table 3. To provide a clearer comparison, the 2PA spectra of the chromophores are presented in Fig. 4. In comparison with the experimental results, it should be noticed that the δ_{max} values of molecules **P1** (2023.3 GM at 725.9 nm), **P2** (1600 GM at 757.9 nm), and **P3** (2207.4 GM at 723.4 nm) are larger by 500 GM than those of the experimental data (1354 GM, 1042 GM, and 1716 GM at 760 nm),[25] respectively. Molecule **P4** exhibits slightly smaller δ_{max} (1233.2 GM) at 780.8 nm than the experimental value (1484 GM). It is reported that the experimental uncertainty on δ_{max} is on the order of 10–15%.[25] Of course, when we consider the experimental uncertainty, the calculated values by ZINDO/SOS almost match with the experiment. While solvent impact on the 2PA properties was taken into account by the PCM model, calculations of δ_{max} in THF are carried out as well (*cf.* Table 3). In general, the solvent effects on 2PA properties are very slight with respect to those in gas phase except for **P4** and **P7**: for instance, the strongest peaks of 2PA wavelength are almost unchanged; the δ_{max} values are slightly reduced or enhanced. Although the λ^{T}_{max} values in THF of **P4** and **P7** are red-shifted by 15 nm and their δ_{max} in THF are reduced by 30% than those in gas. Nevertheless, the relative changing rules keep almost the same both in gas phase and in THF. Additionally, for the sake of clearer comparison, we take molecules **P2** and **P4** as examples to calculate their 2PA cross sections using the response theory at DFT//CAM-B3LYP/6-31G* level implemented in DALTON2011.[45,46] From Table 3, it can be observed that the maximum 2PA cross sections of the two tested molecules are 121.4 GM and 325.7 GM at 782.2 nm and 659.5 nm, respectively. As compared, the δ_{max} values of **P2** and **P4** by the DFT calculation are much lower than the experimental results (1042 and 1484 GM). Thereafter, the ZINDO method is more appropriate for the studied dyes as previously reported.[47,48]

As shown in Table 3, the maximum values of 2PA spectra are less than twice those of the one photon absorption maximum, proving a quadrupolar character. As shown, all fluorophores exhibit the strongest 2PA band in the near-infrared region and the largest δ_{max} values in the range of 1233.2–10 435.4 GM. This indicates that the *N*-arylpyrrole-based chromophores can be used as excellent two-photon fluorescence labeling materials.

 This journal is © The Royal Society of Chemistry 2012

Published on 30 July 2012 on http://pubs.rsc.org | doi:10.1039/C2OB25916H
Downloaded by University of California - San Diego on 01 September 2012

Table 3 One- and two-photon absorption properties (ZINDO)

Mol.	λ^{O}_{max}/nm	f	Transition character	λ^{T}_{max}/nm	δ_{max}/GM	Transition channel and nature
P1	469.0	3.21	$S_0 \rightarrow S_1(H) \rightarrow (L)60\%$	725.9	2023.3	$S_0 \rightarrow S_1 \rightarrow S_4$ (H − 1) → (L + 2)22%
	468.9[c]	3.21[c]		719.2[c]	2117.3[c]	(H − 1) → (L)16% (H) → (L + 1)11%
	321.9	1.57	$S_0 \rightarrow S_{19}$(H − 4) → (L + 3)24%	760[a]	1354[a]	
			(H − 3) → (L + 4)24%			
P1-a	468.3	3.12	$S_0 \rightarrow S_1(H) \rightarrow (L)60\%$	723.4	1978.0	$S_0 \rightarrow S_1 \rightarrow S_4$ (H − 1) → (L + 2)23%
	324.2	1.58	$S_0 \rightarrow S_{19}$(H − 4) → (L + 3)39%			(H − 1) → (L)16% (H) → (L + 1)11%
			(H − 3) → (L + 4)25%			
P1flu	422.0	2.58	$S_0 \rightarrow S_1(H) \rightarrow (L)68\%$	760.0	848.8	$S_0 \rightarrow S_1 \rightarrow S_2$ (H) → (L + 1)46%
						(H − 1) → (L)31%
P2	467.8	3.32	$S_0 \rightarrow S_1(H) \rightarrow (L)61\%$	757.9	1600	$S_0 \rightarrow S_1 \rightarrow S_4$ (H − 1) → (L + 2)20%
	465.7[c]	3.32[c]		755.1[c]	1574.0[c]	(H − 1) → (L)15%
	283.4	1.08	$S_0 \rightarrow S_{33}$(H − 6) → (L + 3)20%	760[a]	1042[a]	
			(H − 5) → (L + 4)20%	782.2[b]	121.4[b]	
P3	471.2	2.50	$S_0 \rightarrow S_1(H) \rightarrow (L)71\%$	723.4	2207.4	$S_0 \rightarrow S_1 \rightarrow S_4$ (H − 1) → (L)28%
	471.0[c]	2.49[c]		721.7[c]	2058.3[c]	(H) → (L + 1)20% (H − 1) → (L + 4)11%
	321.1	0.84	$S_0 \rightarrow S_{23}$(H − 2) → (L + 1)18%	760[a]	1716[a]	
			(H − 3) → (L)12%			
P4	479.4	2.65	$S_0 \rightarrow S_1(H) \rightarrow (L)71\%$	780.8	1233.2	$S_0 \rightarrow S_1 \rightarrow S_3$ (H, H) → (L, L)12%
	471.3[c]	2.68[c]		796.8[c]	853.8[c]	(H − 1) → (L)38%
	279.9	0.37	$S_0 \rightarrow S_{34}$(H − 5) → (L + 4)14%	760[a]	1484[a]	
			(H − 4) → (L + 1)12%	659.5[b]	325.7[b]	
P5	470.8	3.22	$S_0 \rightarrow S_1(H) \rightarrow (L)61\%$	728.5	2076.9	$S_0 \rightarrow S_1 \rightarrow S_4$ (H − 1) → (L + 2)16%
	470.8[c]	3.22[c]		721.7[c]	2194.8[c]	(H − 1) → (L)14% (H) → (L + 1)10%
	321.8	1.51	$S_0 \rightarrow S_{18}$(H − 4) → (L + 3)27%			
			(H − 3) → (L + 4)20%			
P6	444.0	3.46	$S_0 \rightarrow S_1(H) \rightarrow (L)56\%$	676.0	2207.3	$S_0 \rightarrow S_1 \rightarrow S_7$ (H − 1) → (L + 3)16%
	442.9[c]	3.47[c]		670.2[c]	2390.4[c]	
	312.6	1.66	$S_0 \rightarrow S_{20}$(H) → (L + 1)14%			
			(H − 2) → (L)12%			
P7	448.4	3.23	$S_0 \rightarrow S_4(H) \rightarrow (L + 2)65\%$	720.8	1236.8	$S_0 \rightarrow S_4 \rightarrow S_{14}$ (H − 1) → (L + 2)23%
	436.6[c]	3.31[c]		734.5[c]	789.2[c]	(H) → (L + 3)12% (H − 1) → (L + 4)11%
P8	436.4	3.76	$S_0 \rightarrow S_4(H) \rightarrow (L + 2)56\%$	694.2	1360.3	$S_0 \rightarrow S_4 \rightarrow S_{17}$ (H − 1) → (L + 4)15%
	433.5[c]	3.86[c]	(H − 1) → (L + 3)26%	695.0[c]	1284.5[c]	
P9	640.8	1.26	$S_0 \rightarrow S_1(H) \rightarrow (L)85\%$	1009.7	1547.3	$S_0 \rightarrow S_1 \rightarrow S_2$ (H − 1) → (L)63%
	665.0[c]	0.92[c]		1011.3[c]	1422.6[c]	
	446.8	1.45	$S_0 \rightarrow S_3(H) \rightarrow (L + 1)68\%$	744.2	9409.3	$S_0 \rightarrow S_1 \rightarrow S_6$ (H − 1) → (L + 1)29%
	319.4	0.79	$S_0 \rightarrow S_{32}$(H) → (L + 7)13%	747.8[c]	8872.3[c]	(H,H) → (L,L + 1)19%
			(H − 2) → (L + 2)11%	694.2	10 435.4	$S_0 \rightarrow S_1 \rightarrow S_8$ (H − 5) → (L)23%

[a] Experimental data.[25] [b] DFT results in the DALTON2011 code. [c] Calculation in THF solution.

And the latter section will be devoted to discussing the influence of structural aspects on the 2PA properties.

In general, the position and relative strength of the two-photon resonance could be predicted with the following three-level energy model simplified form of the SOS expression:[11,40,41]

$$\delta \propto \frac{M_{0k}^2 M_{kn}^2}{(E_{0k} - E_{0n}/2)^2 \Gamma} + \frac{M_{0n}^2 \Delta\mu_{0n}^2}{(E_{0n}/2)^2 \Gamma} \quad (5)$$

Here, M_{ij} is the transition dipole moment from the state i to j; E_{ij} is the corresponding excitation energy, the subscripts 0, k, and n refer to the ground state S_0, the intermediate state S_k, and the 2PA final state S_n, respectively; $\Delta\mu_{0n}$ is the state dipole moment difference between S_0 and S_n; the damping factor Γ is set to 0.16 eV. Table 4 lists some important linear absorption parameters for the intermediate and final states of two-photon absorption of studied compounds.

Effect of central core. To assess the influence of the central moiety on the 2PA properties, we compare δ_{max} of **P1** with that of its analogs **P3**, **P5**, **P6**, and **P9**, where the fluorenylene (Flu) moiety at the center is replaced by dimethoxyphenylene, carbazole, pyrene, and benzothiadiazole. From Table 3 and Fig. 4a, it is obvious that fluorophore **P9** is somehow superior to other three molecules in 2PA properties. Specifically, the δ_{max} value of **P9** (9409.3 GM) is 4.7-fold larger than that of molecule **P1** (2023.3 GM) in the near IR region as compared to **P1**, following a bathochromic shift by 283.8 nm of the long 2PA wavelength. It is attributed to the stronger ICT ability of the electron-withdrawing benzothiadiazole incorporated into the π-center. Additionally, **P9** features the lowest energy tuning term ($E_{0k} - E_{0n}/2$) among all molecules (*cf.* Table 4), which is responsible for its highest 2PA cross section.

The introduction of *N*-arylpyrrole moieties leads to the enhancement of the 2PA cross section. Namely, the δ_{max} value of **P1** is 2.5 times higher than that of **P1flu** (848.8 GM). From Table 4, it is noted that introducing the *N*-arylpyrrole moieties can induce the enhancement of M_{kn} (the transition dipole moment between the intermediate state and final state). The result implies that the pyrrole moieties can efficiently increase intramolecular charge transfer, and thereby benefit enhanced δ_{max}. Accordingly, the *N*-arylpyrrole-based derivatives are thought to be promising candidates for the further development of novel 2PA biomolecular labeling materials.

Downloaded by University of California - San Diego on 01 September 2012
Published on 30 July 2012 on http://pubs.rsc.org | doi:10.1039/C2OB25916H

Effect of R groups. Regarding Table 3 and Fig. 4b, it is worth noting that replacement of triphenylamine with phenylene makes the λ^{T}_{max} values show significant bathochromic-shifts, for instance, **P1** (725.9 nm) < **P2** (757.9 nm), and **P3** (723.4 nm) < **P4** (780.8 nm). However, by incorporating boron-dipyrromethene units at the R positions, chromophore **P8** exhibits a hypsochromic shift of the 2PA band with respect to **P1**. When the δ_{max} values of the chromophores with the same core and different *N*-substituted pyrroles are compared, for **P1** and **P2**, the δ_{max} of **P1** is larger than that of **P2**, even as **P3** and **P4** follow the same trend. This can be ascribed to the presence of triphenylamine groups linked to the pyrrole moieties leading to possible multiple pathways for intramolecular electronic and photonic transfer. Hence **P1** features the lower energy tuning term and **P3** possesses the larger M_{kn}. Interestingly, by incorporating boron-dipyrromethene units at the R positions, chromophores **P8** and **P7** exhibit smaller δ_{max} than **P1** and **P3**, respectively. The former should be attributed to **P8** possessing the smallest M_{kn}. The latter can be explained by their structures. As shown in Fig. 2, **P7** features 1,4-dimethoxyphenylene and boron-dipyrromethene moieties which results in the twist structure due to their close proximity. The nonplanar structure hampers ICT and thus decreases δ_{max}. Moreover, the fluorenylene group possesses larger π-electron delocalization and planar structure than the dimethoxyphenylene group and, would increase the electron density, thus benefit ICT between the terminal donor and π-center moieties. In short, it would be a new design strategy to enhance δ_{max} by changing the aromatic rings attached to pyrrole moieties through the C–N bond to modulate the molecular size and intramolecular charge transfer.

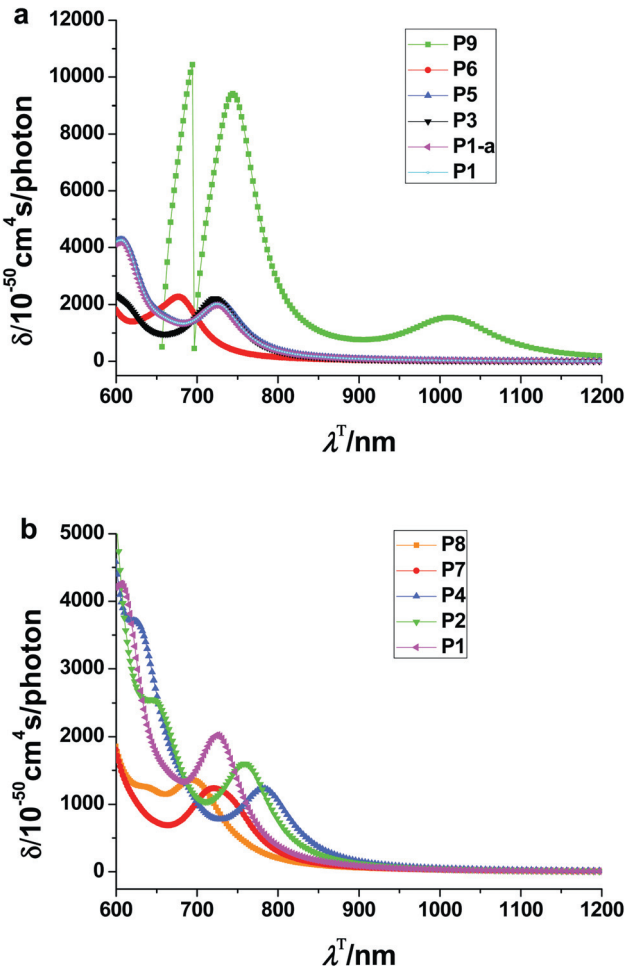

Fig. 4 Two-photon absorption spectra for all the molecules.

In summary, we made structural modifications in order to improve their two-photon optical properties and enlarge the repertoire of their biomolecular target specificity. The present results emphasize the highly versatile potential of **P9** in terms of molecular diversity and of bioimaging.

Conclusions

The systematic investigation of the geometric and electronic structures as well as linear and nonlinear optical properties on such novel *N*-arylpyrrole chromophores is of great significance for both fine-tuning electronic spectra and designing 2PA fluorescent probes. The influence of the π-conjugated center and *N*-substituted pyrrole moieties on OPA and 2PA properties was studied in detail. Introducing *N*-arylpyrrole moieties produces bathochromic-shifts of the absorption and emission bands and an enhancement of the 2PA cross section, which implies that the electron-rich pyrrole moieties can efficiently increase intramolecular charge transfer. Substitution of the fluorenyl center with the benzothiadiazole building block leads to the lower energy gap, red-shifts of OPA and 2PA spectra, higher emission lifetime, and larger 2PA cross section. The aromatic rings attached to pyrrole through the C–N single bond can modulate the absorption in the high energy range and thus subtly modify the opto-electronic properties. Interestingly, the presence of triphenylamine groups

Table 4 Important optical parameters of two-photon absorption for the studied fluorophores

Mol.	Channels	M_{0k}/D	M_{kn}/D	M_{0n}/D	E_{0k}/eV	E_{0n}/eV	$E_{0k} - E_{0n}/2$	$\Delta\mu_{0n}$/D	δ_{max}/GM
P1	$S_0 \rightarrow S_1 \rightarrow S_4$	17.87	13.34	0.83	2.64	3.41	0.935	1.57	2023.3
Pflu	$S_0 \rightarrow S_1 \rightarrow S_2$	15.21	1.61	5.63	2.94	3.31	1.285	1.16	848.8
P2	$S_0 \rightarrow S_1 \rightarrow S_4$	18.17	13.38	1.30	2.65	3.25	1.025	0.77	1600
P3	$S_0 \rightarrow S_1 \rightarrow S_4$	15.80	15.51	1.01	2.63	3.41	0.92	1.63	2207.4
P4	$S_0 \rightarrow S_1 \rightarrow S_3$	16.42	12.80	0.11	2.59	3.16	1.01	0.70	1233.2
P5	$S_0 \rightarrow S_1 \rightarrow S_4$	17.94	12.37	0.79	2.63	3.39	0.935	1.18	2076.9
P6	$S_0 \rightarrow S_1 \rightarrow S_7$	18.06	9.78	0.33	2.79	3.64	0.97	1.17	2207.3
P7	$S_0 \rightarrow S_4 \rightarrow S_{14}$	17.52	11.49	0.51	2.77	3.47	1.035	3.27	1236.8
P8	$S_0 \rightarrow S_4 \rightarrow S_{17}$	18.67	7.90	0.76	2.84	3.61	1.035	1.34	1360.3
P9	$S_0 \rightarrow S_1 \rightarrow S_6$	13.09	13.99	1.24	1.93	3.33	0.265	0.71	9409.3

 This journal is © The Royal Society of Chemistry 2012

linked to the pyrrole moieties leading to possible multiple pathways for intramolecular charge transfer and in turn enhance δ_{max}. In the present study, the structural modifications are successful to improve the OPA and 2PA properties of the *N*-arylpyrrole-based chromophores and enlarge the repertoire of their practical applications. In general, they exhibit interesting opto-electronic behaviors, which would be potential candidates for excellent two-photon fluorescence labeling materials. The present work would help guiding the synthesis towards the most promising derivatives.

Acknowledgements

This work is supported by the Natural Science Foundation of China (No. 20973078 and 21173099), and Special Funding to Basic Scientific Research Projects for Central Collages. We thank the referees for invaluable suggestions and comments.

Notes and references

1 M. Göppert-Mayer, *Ann. Phys.*, 1931, **401**, 273–294.
2 W. Kaiser and C. G. B. Garrett, *Phys. Rev. Lett.*, 1961, **7**, 229–231.
3 W. R. Zipfel, R. M. Williams and W. W. Webb, *Nat. Biotechnol.*, 2003, **21**, 1369–1377.
4 J.-F. Xing, X.-Z. Dong, W.-Q. Chen, X.-M. Duan, N. Takeyasu, T. Tanaka and S. Kawata, *Appl. Phys. Lett.*, 2007, **90**(13), 131106.
5 S. Kawata and Y. Kawata, *Chem. Rev.*, 2000, **100**, 1777–1788.
6 P. A. Bouit, G. Wetzel, G. Berginc, B. Loiseaux, L. Toupet, P. Feneyrou, Y. Bretonnière, K. Kamada, O. Maury and C. Andraud, *Chem. Mater.*, 2007, **19**, 5325–5335.
7 J. Arnbjerg, A. Jiménez-Banzo, M. J. Paterson, S. Nonell, J. I. Borrell, O. Christiansen and P. R. Ogilby, *J. Am. Chem. Soc.*, 2007, **129**, 5188–5199.
8 T. C. Lin, S. J. Chung, K. S. Kim, X. Wang, G. S. He, J. Swiatkiewicz, H. E. Pudavar and P. N. Prasad, *Adv. Polym. Sci.*, 2003, **161**, 157–193.
9 (*a*) O. Opanasyuk, L. Ryderfors, E. Mukhtar and L. B.-Å. Johansson, *Phys. Chem. Chem. Phys.*, 2009, **11**, 7152–7160; (*b*) Y. H. Zhang, J. J. Wang, P. F. Jia, X. Q. Yu, H. Liu, X. Liu, N. Zhao and B. B. Huang, *Org. Biomol. Chem.*, 2010, **8**, 4582–4588; (*c*) X. Liu, Y. M. Sun, Y. H. Zhang, F. Miao, G. C. Wang, H. S. Zhao, X. Q. Yu, H. Liu and W.-Y. Wong, *Org. Biomol. Chem.*, 2011, **9**, 3615–3618.
10 M. Pawlicki, H. A. Collins, R. G. Denning and H. L. Anderson, *Angew. Chem., Int. Ed.*, 2009, **48**, 3244–3266.
11 M. Rumi, J. E. Ehrlich, A. A. Heikal, J. W. Perry, S. Barlow, Z. Y. Hu, D. McCord-Maughon, T. C. Parker, H. Rockel, S. Thayumanavan, S. R. Marder, D. Beljonne and J. L. Bredas, *J. Am. Chem. Soc.*, 2000, **122**, 9500–9510.
12 C. Katan, M. Charlot, O. Mongin, C. Le Droumaguet, V. Jouikov, F. Terenziani, E. Badaeva, S. Tretiak and M. Blanchard-Desce, *J. Phys. Chem. B*, 2010, **114**, 3152–3169.
13 B. R. Cho, K. H. Son, S. H. Lee, Y. S. Song, Y. K. Lee, S. J. Jeon, J. H. Choi, H. Lee and M. H. Cho, *J. Am. Chem. Soc.*, 2001, **123**, 10039–10045.
14 F. Terenziani, V. Parthasarathy, A. Pla-Quintana, T. Maishal, A. M. Caminade, J. P. Majoral and M. Blanchard-Desce, *Angew. Chem., Int. Ed.*, 2009, **48**, 8691–8694.
15 P. C. Jha, Y. Wang and H. Ågren, *ChemPhysChem*, 2008, **9**, 111–116.
16 M. M. Alam, M. Chattopadhyaya and S. Chakrabarti, *Phys. Chem. Chem. Phys.*, 2011, **13**, 9285–9292.
17 P. Shao, B. Huang, L. Q. Chen, Z. J. Liu, J. G. Qin, H. M. Gong, S. Ding and Q. Q. Wang, *J. Mater. Chem.*, 2005, **15**, 4502–4506.
18 A. Abbotto, L. Beverina, R. Bozio, A. Facchetti, C. Ferrante, G. A. Pagani, D. Pedron and R. Signorini, *Org. Lett.*, 2002, **4**, 1495–1498.
19 S. J. Zheng, L. Beverina, S. Barlow, E. Zojer, J. Fu, L. A. Padilha, C. Fink, O. Kwon, Y. P. Yi, Z. G. Shuai, E. W. Van Stryland, D. J. Hagan, J. L. Bredas and S. R. Marder, *Chem. Commun.*, 2007, 1372–1374.
20 V. Hrobáriková, P. Hrobárik, P. Gajdoš, I. Fitilis, M. Fakis, P. Persephonis and P. Zahradník, *J. Org. Chem.*, 2010, **75**, 3053–3068.
21 L. Beverina, J. Fu, A. Leclercq, E. Zojer, P. Pacher, S. Barlow, E. W. V. Stryland, D. J. Hagan, J. L. Brédas and S. R. Marder, *J. Am. Chem. Soc.*, 2005, **127**, 7282–7283.
22 S. J. Chung, S. Zheng, T. Odani, L. Beverina, J. Fu, L. A. Padilha, A. Biesso, J. M. Hales, X. Zhan, K. Schmidt, A. J. Ye, E. Zojer, S. Barlow, D. J. Hagan, E. W. Stryland, V. Y. P. Yi, Z. G. Shuai, G. A. Pagani, J. L. Brédas, J. W. Perry and S. R. Marder, *J. Am. Chem. Soc.*, 2006, **128**, 14444–14445.
23 S. Zheng, A. Leclercq, J. Fu, L. Beverina, L. A. Padilha, E. Zojer, K. Schmidt, S. Barlow, J. Luo, S. Jiang, A. K. Y. Jen, Y. Yi, Z. G. Shuai, E. W. V. Stryland, D. J. Hagan, J. L. Brédas and S. R. Marder, *Chem. Mater.*, 2007, **19**, 432–442.
24 Q. Li, C. Lu, J. Zhu, E. Fu, C. Zhong, S. Li, Y. Cui, J. Qin and Z. Li, *J. Phys. Chem. B*, 2008, **112**, 4545–4551.
25 Q. Q. Li, J. Huang, A. S. Zhong, C. Zhong, M. Peng, J. Liu, Z. G. Pei, Z. L. Huang, J. G. Qin and Z. Li, *J. Phys. Chem. B*, 2011, **115**, 4279–4285.
26 P. Conlon, C. J. Yang, Y. Wu, Y. Chen, K. Martinez, Y. Kim, N. Stevens, A. A. Marti, S. Jockusch, N. J. Turro and W. Tan, *J. Am. Chem. Soc.*, 2008, **130**, 336–342.
27 M. Drobizhev, N. S. Makarov, S. E. Tillo, T. E. Hughes and A. Rebane, *Nat. Methods*, 2011, **8**, 393–399.
28 S. Biswas, X. H. Wang, A. R. Morales, H.-Y. Ahn and K. D. Belfield, *Biomacromolecules*, 2011, **12**, 441–449.
29 A. S. Rao, D. Kim, T. Wang, K. H. Kim, S. Hwang and K. H. Ahn, *Org. Lett.*, 2012, **14**, 2598–2601.
30 P. Hanczyc, B. Nordena and M. Samoc, *Dalton Trans.*, 2012, **41**, 3123–3125.
31 N. M. F. S. A. Cerqueira, P. A. Fernandes, L. A. Eriksson and M. J. Ramos, *J. Comput. Chem.*, 2004, **25**, 2031–2037.
32 T. Yanai, D. P. Tew and N. C. Handy, *Chem. Phys. Lett.*, 2004, **393**, 51–57.
33 Y. Zhao and D. G. Truhlar, *Theor. Chem. Acc.*, 2008, **120**, 215–241.
34 W. P. Anderson, W. D. Edwards and M. C. Zerner, *Inorg. Chem.*, 1986, **25**, 2728–2732.
35 M. J. Frisch, G. W. Trucks and H. B. Schlegel, *et al.*, *GAUSSIAN 09 (Revision B.01)*, Gaussian Inc., Wallingford, CT, 2010.
36 M. Cha, W. E. Torruellas, G. I. Stegeman, W. H. G. Horsthuis, G. R. Möhlmann and J. Meth, *Appl. Phys. Lett.*, 1994, **65**, 2648–2650.
37 T. Kogej, D. Beljonne, F. Meyers, J. W. Perry, S. R. Marder and J. L. Brédas, *Chem. Phys. Lett.*, 1998, **298**, 1–6.
38 B. J. Orr and J. F. Ward, *Mol. Phys.*, 1971, **20**, 513–526.
39 D. M. Bishop, J. M. Luis and B. Kirtman, *J. Chem. Phys.*, 2002, **116**, 9729–9379.
40 D. Beljonne, W. Wenseleers, E. Zojer, Z. Shuai, H. Vogel, S. J. K. Pond, J. W. Perry, S. R. Marder and J. L. Brédas, *Adv. Funct. Mater.*, 2002, **12**, 631–641.
41 M. Albota, D. Beljonne, J. L. Brédas, J. E. Ehrlich, J. Y. Fu, A. A. Heikal, S. E. Hess, T. Kogej, M. D. Levin, S. R. Marder, D. McCord-Maughor, J. W. Perry, H. Röckel, M. Rumi, G. Subramaniam, W. W. Webb, X. L. Wu and C. Xu, *Science*, 1998, **281**, 1653–1656.
42 I. Litani-Barzilai, V. Bulatov and I. Schechter, *Anal. Chim. Acta*, 2004, **501**, 151–156.
43 V. Lukeš, A. Aquino and H. Lischka, *J. Phys. Chem. A*, 2005, **109**, 10232–10238.
44 B. Carlson, G. D. Phelan, W. Kaminsky, L. Dalton, X. Z. Jiang, S. Liu and A. K. Y. Jen, *J. Am. Chem. Soc.*, 2002, **124**, 14162–14172.
45 *DALTON, A Molecular Electronic Structure Program*, Release Dalton2011 (2011), see http://daltonprogram.org/
46 M. Chattopadhyaya, M. M. Alam and S. Chakrabarti, *J. Phys. Chem. A*, 2011, **115**, 2607–2614.
47 X.-T. Liu, L.-Y. Zou, A.-M. Ren, J.-F. Guo, Y. Sun, S. Huang and J.-K. Feng, *Theor. Chem. Acc.*, 2011, **130**, 37–50.
48 X.-T. Liu, J.-F. Guo, A.-M. Ren, S. Huang and J.-K. Feng, *J. Org. Chem.*, 2012, **77**, 585–597.

Published on 30 July 2012 on http://pubs.rsc.org | doi:10.1039/C2OB25916H
Downloaded by University of California - San Diego on 01 September 2012